Inorg. Chem. **2007**, *46*, 2645–2658

Steric and Electronic Effects Relating to the Cu^{2+} Jahn–Teller Distortion in $Zn_{1-x}Cu_xAl_2O_4$ Spinels§

A. Le Nestour,† M. Gaudon,† G. Villeneuve,† R. Andriessen,‡ and A. Demourgues*,†

Institut de Chimie de la Matière Condensée, UPR 9048 CNRS, Université de Bordeaux I, 87 avenue du Dr A. Schweitzer 33608 Pessac Cedex, France, and Agfa-Gevaert, Septestraat 27 − B-2640 Mortsel, Belgium

Received December 6, 2006

$Zn_{1-x}Cu_xAl_2O_4$ ($0 \leq x \leq 1$) compositions have been synthesized by solid-state route, and a color scale going from white ($x = 0$) to brownish-red ($x = 1$) with intermediate colors as pale green for $x = 0.10$ and pale brown for $x = 0.30$ can be observed. XRD-data refinements on the whole solid solution have allowed defining two critical areas where structural features such as cell parameter and inversion rate as well as cation-oxygen bond distances in 8a and 16d sites of the spinel network exhibit clear unique variations. By observing the direct environment of tetrahedral and octahedral sites potentially occupied by Cu^{2+} Jahn–Teller cations, the two critical compositions have been estimated to $x_1 = 1/6$ and $x_2 = 4/7$. Actually from the x_1 and x_2 copper contents, the probability of getting Cu^{2+}–Cu^{2+} pairs involving tetrahedral-octahedral or two octahedral sites respectively is high. Then, the stabilization of Cu^{2+} JT ions in distorted octahedral site, identified by ESR, is in competition with the occurrence of Cu^{2+} in tetrahedral sites, and both electronic and steric effects of Cu^{2+} JT cations lead to the explanation of the evolution of the inversion rate in this series. The study of the optical absorption properties clearly shows that the position and the intensity of the various absorption bands are influenced by the distribution of Cu^{2+} ions in tetrahedral and octahedral sites, the creation of Cu^{2+}–Cu^{2+} pairs around the x_1 and x_2 critical compositions, and the increasing of Cu–O bond covalency. Such an evolution of structural features correlated with electronic properties where various critical compositions have been identified can be generalized to other spinel oxides, considering local distortion around Jahn–Teller ions.

Introduction

Cu-based oxides have been studied and developed for the two last decades, because of their relevant electronic properties mentioned for instance in the case of high Tc superconductors. On a fundamental point of view, the stabilization of Cu^{2+} Jahn−Teller (JT) ions in a distorted octahedral site, square planes (D_{4h}), or square pyramidal environment (C_{4v}) governs the distribution of $\sigma^*_{x^2-y^2}$ antibonding and σ_z^2 bonding orbitals and the occurrence of a strong Cu/O coupling or charge transfer into the basal plane.[1−3] This leads to a large number of charge carriers delocalized in a conduction band and to a metallic or superconducting behavior. Another example concerns the case of delafossite structure $CuAlO_2$ where defects can be stabilized at the origin of the p-type semiconducting behavior of this transparent conductive oxide (TCO).[4]

Actually, the Cu^{2+} JT distortion can be cooperative or only affects several sites into the network without any evolution of the symmetry of the crystal structure. Thus in the spinel network, where Cu^{2+} can be easily stabilized both in distorted octahedral and tetrahedral environments, various cases have been observed. For instance for larger transition cations such as Cr^{3+} ($3d^3$) or Fe^{3+} ($3d^5$) ions which exhibit a capability to be distorted, a tetragonal symmetry $I4_1/amd$ derived from the spinel structure is observed at room temperature for Cu-

* To whom correspondence should be addressed. E-mail: demourg@icmcb-bordeaux.cnrs.fr.
† Université de Bordeaux I.
‡ Agfa-Gevaert.

§ This paper is dedicated to Prof. Gérard Villeneuve who passed away the 28th of January 2007.

(1) Bianconi, A.; Congiu-Castallano, A.; De Santis, M.; Delagu, P.; Gargano, A.; Giordi, R. *Solid State Commun.* **1987**, *63*, 1135.
(2) Hinks, D. G.; Dabrowski, B.; Jorgensen, J. D.; Mitchell, A. W.; Richards, D. R.; Pei, S.; Shi, D. *Nature* **1988**, *333*, 836.
(3) Pouchard, M.; Grenier, J. C.; Doumerc, J. P.; Demazeau, G.; Chaminade, J. P.; Wattiaux, A.; Dordor, P.; Hagenmuller, P. *Mater. Res. Soc. Symp. Proc.* **1989**, *156*.
(4) Ingram, B. J.; Gonzalez, G. B.; Mason, T. O.; Shahriari, D. Y.; Barnabè, A.; Ko, D.; Poeppelmeier, K. R. *Chem. Mater.* **2004**, *16*, 5616−5622.

10.1021/ic062329c CCC: $37.00
Published on Web 02/10/2007

$[Cr_2]O_4$ and $Fe[CuFe]O_4$ compositions[5,6] where cations in brackets are located in octahedral sites. In both of these last structures, Cu^{2+} cations can be stabilized in flattened tetrahedral sites and an elongated octahedral environment, respectively, because of the preference of Cr^{3+} ions to occupy octahedral sites and the absence of the coordination's preference of Fe^{3+} ions. In $Cu[MnCr]O_4$ and $Fe[CuMn]O_4$ compounds,[7] Mn^{3+} (d^4) are substituting for half of the Cr^{3+} or the Fe^{3+} ions and are stabilized in a distorted octahedral site thanks also to a JT effect. The symmetry of these two compositions becomes cubic with the *Fd*-3*m* space group at room temperature. In the $CuMn_2O_4$ compound, the mixed valencies states of Cu and Mn lead to a distribution of transition metals in tetrahedral and octahedral sites and the symmetry of the spinel network remains cubic.[8] In both of these last examples, the presence of Mn^{3+} contributes to removing the cooperative JT distortion, and a distribution of Cu^{2+} cations in both tetrahedral and octahedral sites can be considered in the spinel network. In the case of Ga^{3+} ($3d^{10}$) ions whose electronegativity becomes higher and ionic radius is comparable to that of Cr^{3+} ions, the local polarizing effect becomes more and more important and the $Ga[CuGa]O_4$ compound keeps the cubic *Fd*-3*m* symmetry of the spinel structure.[9] In this example, one should also have to notice the possibility of getting Cu^{2+} ions both in tetrahedral and octahedral sites leading to a vanishing of the cooperative JT distortion. Moreover it seems to be difficult to produce a cooperative JT distortion because isotropic Ga^{3+} ($3d^{10}$) ions do not support strong constrains. Finally in $Zn[CuTi]O_4$ composition,[9] the presence of Ti^{4+} ions, which exhibits a strong polarizing character, contributes in the same way to a disappearance of the cooperative JT distortion.

This work deals with the structural investigations of the $Zn_{1-x}Cu_xAl_2O_4$ solid solution and the relationships with optical absorption properties in the UV−vis-NIR range. Starting from a partial XRD data refinement and Monte Carlo calculation, C. Otero Arean et al.[10] had already refined the inversion rate in these series, but the authors conclude that such cations distribution does not agree with thermodynamic arguments and especially enthalpies values. For instance in $CuAl_2O_4$, XRD data refinements showed that 35% of Cu^{2+} occupies octahedral sites, whereas thermodynamic considerations and calculations demonstrate the opposite effect with 65% of Cu^{2+} in octahedral symmetry.

Other routes have been attempted to prepare divided zinc−copper aluminates based on the polyesterification reaction implying metallic salts followed by an annealing at low temperatures and have been described in a forthcoming paper.[11] By this method, defects corresponding to oxygen vacancies and various Cu oxidation states, Cu^{+I}/Cu^{+II}, have been stabilized into the spinel framework.[11] One should have to note that low temperatures hydrothermal techniques lead also to the stabilization of defects (Al_{Cu}-"$2O_i$") in $CuAlO_2$−TCO− with Al in the Cu site and interstitial oxygen ions forming a pseudotetrahedral site around Cu environments.[4]

The series prepared by a solid-state route at high temperatures has been first studied by Rietveld refinement of XRD data leading to determine accurately the cell parameter, the inversion rate, and the metal−oxygen bond distances. Various critical regions with defined *x* values will be discussed on the basis of geometrical considerations taking into account electronic and steric effects of JT Cu^{2+} ions. ESR and magnetic measurements have been performed in order to get information about the local environment and the valence of Cu cations. Finally, the UV−vis-NIR optical absorption properties governed by the Cu content as well as the inversion rate and the Cu−O bond distances will be discussed.

Experimental Section

1. Preparation of Compounds and Chemical Analysis. $Zn_{1-x}Cu_xAl_2O_4$ compositions with $0 \leq x \leq 1$ and references Cu-doped magnesium oxide and Cu-doped zinc oxide were prepared by the conventional solid-state route, starting from binary oxides of high purity in stoichiometric amounts. The mixtures are heated at 1000 °C during 12 h and slowly cooled down. Several grinding and annealing are necessary to obtain pure phases. Chemical compositions have been controlled by microprobe analysis.

2. X-ray Diffraction Analysis. Powder X-ray diffraction patterns have been collected on a Philips X'Pert MPD X-ray diffractometer with a Bragg−Brentano geometry and using Cu $K\alpha_{1,2}$ radiation ($5 < 2\theta < 120°$, step: 0.02° and counting time of 30 s). Diffractogramms have been refined using the Rietveld method with the conventional reliability factors. The Fullprof program package was used. Unit cell parameters atomic positions, occupancies, and Debye−Waller factors have been refined on the basis of the *Fd*-3*m* space group corresponding to the spinel structure.

3. ESR Measurements. Electronic spin resonance spectra have been recorded at room temperature and at 5 K with a Bruker ESR 300E a spectrophotometer in the X-band (9.45 GHz) in order to identify the local environments of Cu^{2+} ions.

4. Magnetic Measurements. Magnetic measurements (magnetizations) have been performed on a S.Q.U.I.D detector magnetometer Quantum Design MPMS 5, between $T = 25$ K and $T = 200$ K with an increment of 50 K, and for applied fields comprised between 0 and 50000 Oe. As Curie constants are proportional to the concentration of paramagnetic species, Cu^{2+} concentration in the various compounds can be deduced from magnetic data.

5. Diffuse Reflectance Spectroscopy. Diffuse reflectance spectra (*R*) have been recorded using a Cary 5E spectrophotometer, with the $210 < \lambda < 2500$ nm range. Halon and MgO standards have been used as references.

Results and Discussion

1. Cationic Distribution into the Spinel Network and Evolution of Structural Features in the $Zn_{1-x}Cu_xAl_2O_4$

(5) Dollase, W. A.; O'Neill, H. S. C. *Acta Crystallogr., Sect. C: Cryst. Struct. Commun.* **1997**, *C53*, 657−659.
(6) Prince, E.; Treuting, R. G. *Acta Crystallogr., Sect. C: Cryst. Struct. Commun.* **1956**, *9*, 1025.
(7) Kulkarni, D. K.; Mande, C. *Indian J. Pure Appl. Phys.* **1974**, *12*, 60−63.
(8) Waskowska, A.; Gerward, L.; Staun, Olsen, J.; Steenstrup, S.; Talik, E. *J. Phys.: Condens. Matter* **2001**, *13*, 2562.
(9) Robbins, M.; Darcy, L. *J. Phys. Chem. Solids* **1966**, *27*, 741−743.
(10) Otero Arean, C.; Diez Vinuela, J. S.; Rubio Gonzalez, J. M.; Mata Arjona, A. *Mater. Chem.* **1981**, *6*, 165−174.
(11) Le Nestour, A.; Gaudon, M.; Villeneuve, G.; Daturi, M.; Andriessen, R.; Demourgues, A. Submitted to *Inorg. Chem.*

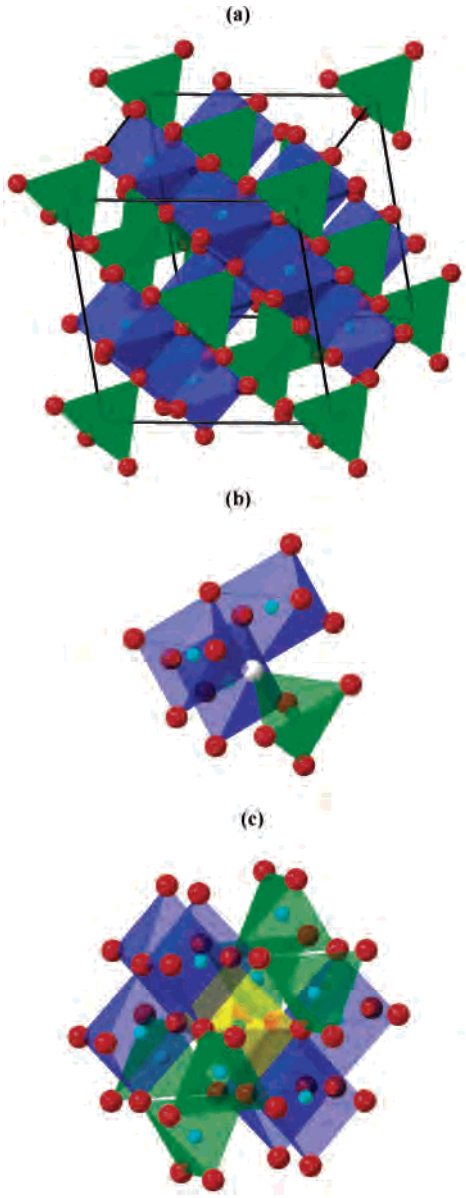

Figure 1. Representation of the spinel structure ($MgAl_2O_4$): whole lattice (a), direct environment of one tetrahedral site (b), and direct environment of one octahedral site (c).

Series. $Zn_{1-x}Cu_xAl_2O_4$ phases ($0 \leq x \leq 1$) adopt a cubic symmetry with the *Fd*-3*m* space group related to the spinel type-structure (Figure 1a). The environment of oxygen surrounded by three octahedra and one tetrahedron as well as the first polyhedra nearest neighbors of octahedral and tetrahedral sites is also represented in Figure 1b,c. Rietveld refinements (experimental, theory, and difference) have been represented in Figure 2a−c for $x = 0$ (a), $x = 0.30$ (b), and $x = 1$ (c). The zinc atoms occupy preferentially the 8a site (tetrahedral site), whereas copper and alumina atoms are distributed between the 8a site and the 16d site (octahedral site). Oxygen atoms are located in the 32e site (u,u,u). The powders X-ray diffractogramms of $Zn_{1-x}Cu_xAl_2O_4$ phases have been refined by the Rietveld method in order to determine accurately the oxygen positions. The conditions of data collection have been detailed in Table 1. The atomic positions, isotropic thermal displacements, occupancies of each site, and reliability factors (R_p, R_{wp}, R_B) for $x = 0$, $x = 0.10$, $x = 0.30$, $x = 0.70$, and $x = 1.00$ are given in Table 2.

$ZnAl_2O_4$ is a direct spinel where Zn^{2+} cations occupy only tetrahedral site (8a), Al^{3+} cations being into octahedral sites (16d), and is described in this manner or as a slightly inverted spinel whatever the synthesis route in the literature.[12,13,27] ^{27}Al QMAS NMR does not reveal any Al^{3+} cation in the tetrahedral environment for as prepared $ZnAl_2O_4$. So, Zn^{2+} ion has to be considered in the tetrahedral site. However the preparation of zinc aluminates from metallic salts at low temperatures leads to a low content of Al^{3+} ions stabilized in tetrahedral sites confirmed by a ^{27}Al QMAS NMR study.[11] When Cu^{2+} cations are introduced into the spinel network, they can be stabilized either in the octahedral or the tetrahedral sites, but their preference goes to octahedral symmetry[14] and strong Jahn−Teller distortion. As Cu^{2+} cations are located in the octahedral site, an equivalent amount of Al^{3+} cations goes to the tetrahedral ones. The spinel network is in this case characterized by its γ inversion rate, corresponding to the content of divalent cations occupying octahedral sites.

The *a* lattice parameter (Figure 3) decreases continuously as a function of the copper rate *x* in the spinel $Zn_{1-x}Cu_xAl_2O_4$ from $a = 8.0861$ (2) Å for $x = 0$ to $a = 8.0784$ (2) Å for $x = 1.00$. The electronic configuration of Cu^{2+} cation is (3d)-$t_2^6e^34s^0$ in octahedral symmetry and (3d) e^4 $t_2^54s^0$ in tetrahedral environment. A strong Jahn−Teller effect is commonly observed for Cu^{2+} cations in octahedral coordination. The ionic radii of Zn^{2+} and Cu^{2+} cations are close. Nevertheless the lattice parameter contraction observed in the solid solution $Zn_{1-x}Cu_xAl_2O_4$ can be explained by the polarizing effect of Cu^{2+} enhanced by the Jahn−Teller distortion. Consequently the increase of the hybridization via the formation of Cu−O bonds contributes to a slight decrease of average cell parameters. However the evolution seems not to be monotonous as shown in Figure 3. The lattice contraction is indeed more pronounced above $x = 0.60$, and this tendency will be discussed later. In the same figure is also reported the evolution of the oxygen parameter *u*, which decreases as the copper content *x* in $Zn_{1-x}Cu_xAl_2O_4$. For compounds prepared at lower temperatures from metallic salts, the *a* cell parameter remains always lower than one determined for homologous compounds with the same *x* Cu content obtained by the solid-state route at $T = 1000$ °C. This tendency can be explained by the creation of defects associated with oxygen vacancies and mixed Cu valence states stabilized in the spinel network.[11]

γ inversion rate values are obtained thanks to XRD data refinement by the Rietveld method with very good discernment, especially represented by the two special diffraction lines (400 and 331) whose intensities ($F^2_{400} = (4f_O + (2-2\gamma)f_{Al}^{3+} + (2\gamma\text{-}1)f_M^{2+})^2$ and $F^2_{331} = [-\sqrt{2}/2((1\text{-}\gamma)f_M^{2+} + \gamma$

(12) Van der Laag, N. J.; Snel, M. D.; Magusin, P. C. M. M.; De With, G. *J. Eur. Ceram. Soc.* **2004**, *24*, 2417−2424.
(13) Cooley, R. F.; Reed, J. S. *J. Am. Ceram. Soc.* **1972**, *55*, 395−398.
(14) Burns, R. G. *Mineralogical applications of crystal field theory*; Syndics of the Cambridge University Press: 1970.

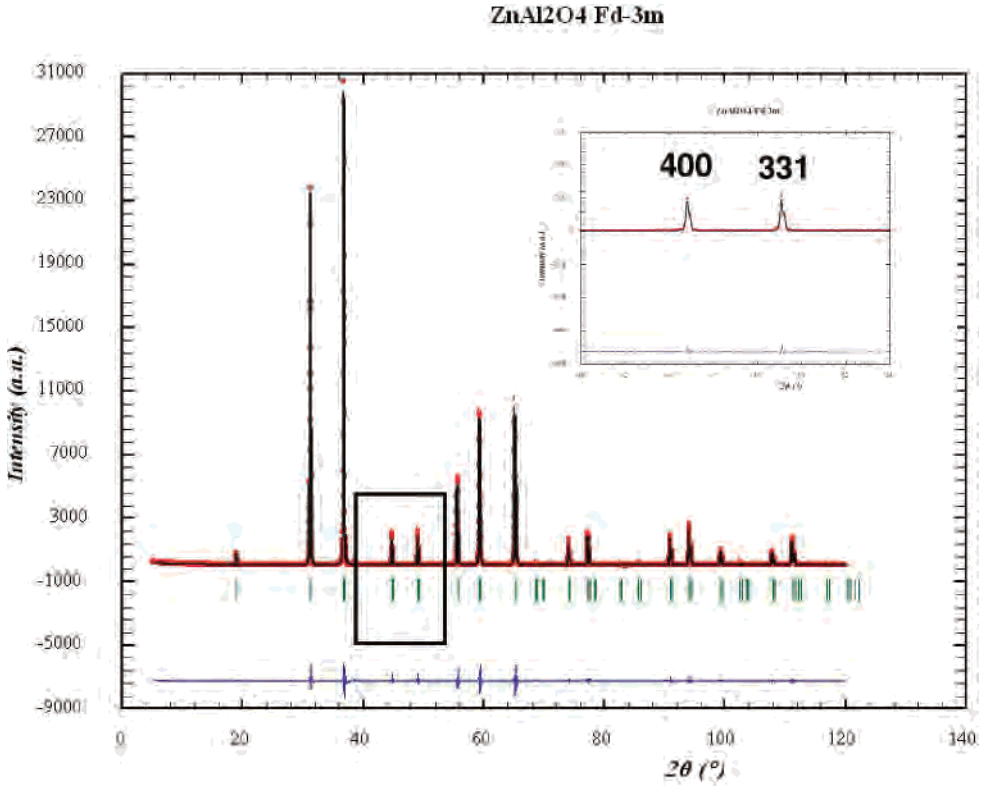
ZnAl2O4 Fd-3m
400
331
Intensity (a.u.)
2θ (°)

(a)

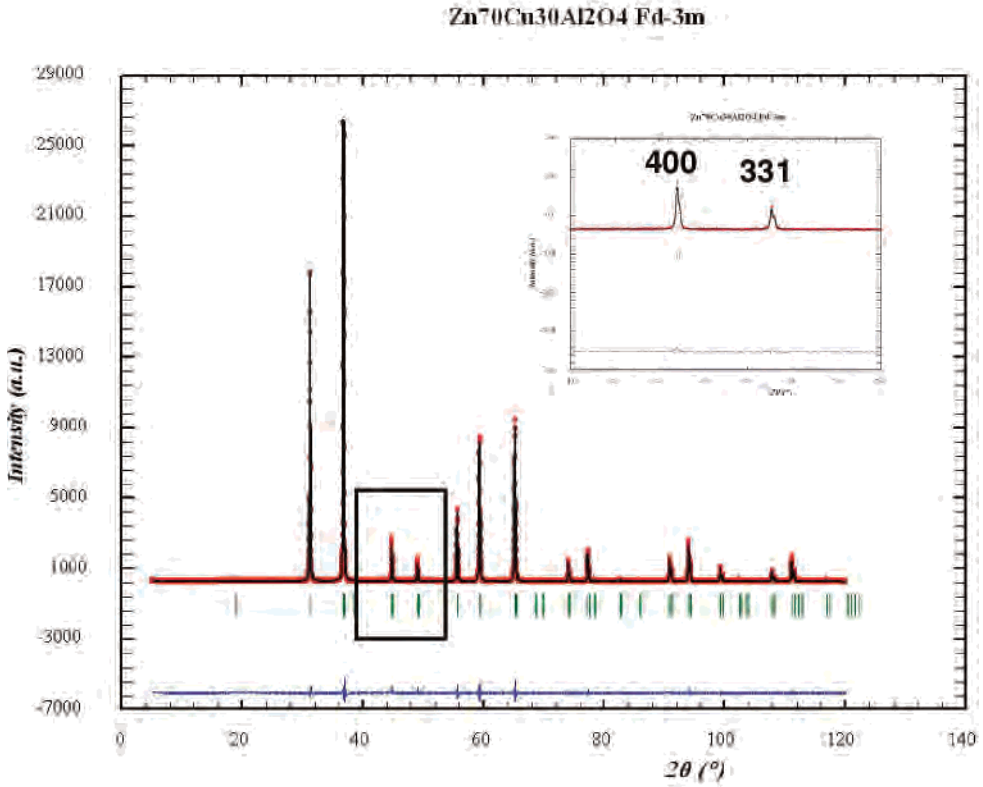
Zn70Cu30Al2O4 Fd-3m
400
331
Intensity (a.u.)
2θ (°)

(b)

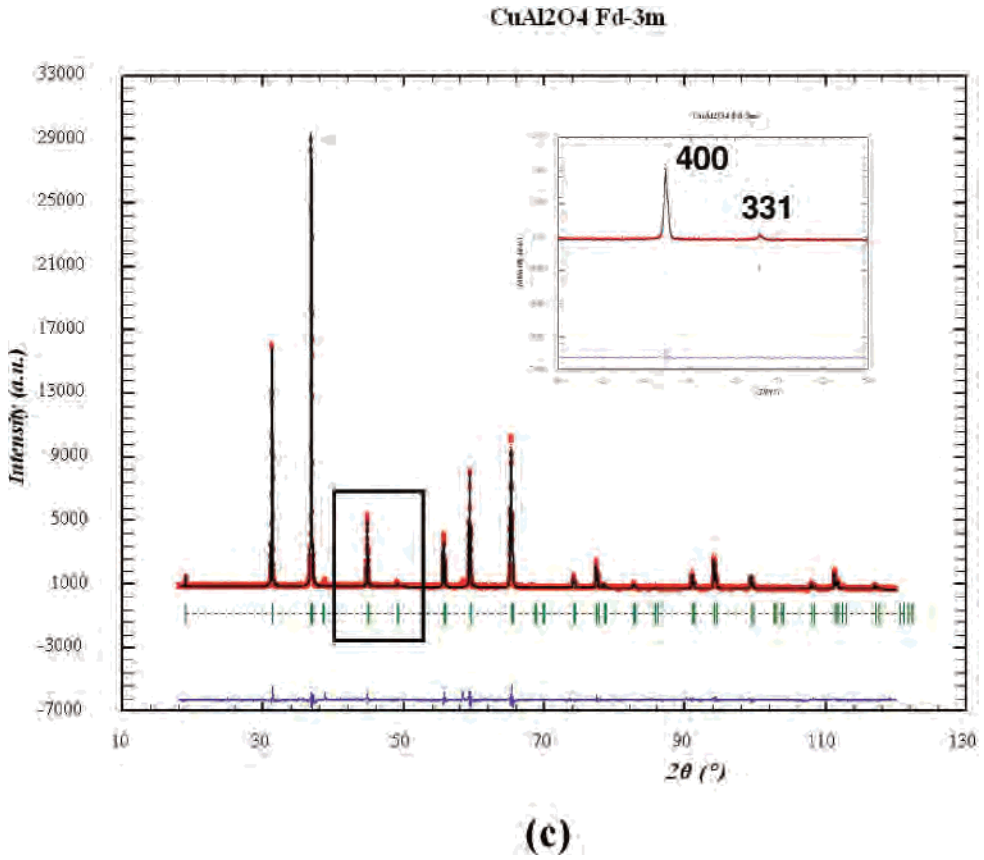

Figure 2. Rietveld refinements of (a) $ZnAl_2O_4$, (b) $Zn_{0.70}Cu_{0.30}Al_2O_4$, and (c) $CuAl_2O_4$ compositions.

Table 1. Rietveld Parameters and Experimental Conditions for Data Collection

formula	AB_2O4
symmetry	cubic
reflection conditions	$h + k = 2n$; $k + l = 2n$; $l + k = 2n$
space group	*Fd*-3*m* (no. 227)
radiation	Cu ($K_{\alpha1}$,$K_{\alpha2}$)
peak shape function	$PV = \eta L + (1-\eta)G$
measuring range (°)	$5° < 2\theta < 120°$
reflections collected	33
parameters used in refinement	20

f_{Al}^{3+}) + (2-γ)f_{Al}^{3+} + γ f_M^{2+}]^2) are very sensitive to the presence of copper cations in octahedral sites (see the zone enlargements in Figure 2a−c). The calculation of their relative intensities and of their relative structure factors for various simulated inversion rates confirms the global refinement and the standard deviation of the refined γ inversion rate (see Table 3 the case of $Zn_{0.70}Cu_{0.30}Al_2O_4$).

The evolution of the inversion rate versus the copper rate x in the spinel $Zn_{1-x}Cu_xAl_2O_4$ is described in Figure 4. The γ inversion rate increases from 0 to 0.35 as the copper rate x in the spinel increases from 0 to 1. The inversion rate is around 18% for $Zn_{0.60}Cu_{0.40}Al_2O_4$ and around 27% for $Zn_{0.40}Cu_{0.60}Al_2O_4$. If zinc cations are assumed to be preferentially stabilized in tetrahedral sites, one should have to note that for compositions comprised between $0.10 \leq x \leq 0.60$, the inversion rate is roughly equal to $x/2$, and in these conditions the copper cations are half distributed in tetrahedral and in octahedral sites. Actually, for compositions with $x < 0.60$, the inversion rate raises regularly and slows down up to $x = 0.60$. As far as the zinc−copper aluminates prepared at low temperatures from metallic salts are concerned, the γ inversion rate, refined on the basis of X-ray diffraction data, remains the same as the one determined for homologous compositions obtained by the solid-state route at high temperatures.[11]

Rietveld refinements give also access to the accurate atomic position of oxygen atoms (Table 2) and consequently to average values of the bond lengths (Table 4) between oxygen atoms (general position 32 e (u,u,u)) and cations (Al^{3+} or Cu^{2+}) in the Oh site (16d (1/2, 1/2, 1/2)) and between oxygen atoms and cations (Al^{3+} or Zn^{2+}) in the tetrahedral site (8a ($^1/_8$,$^1/_8$,$^1/_8$)). A gradual decrease of the u coordinated for O (u,u,u) atoms is observed as the copper rate x increases. One should have to notice whatever the refined O atomic positions, the octahedra and tetrahedra remain almost regular. For instance for $Zn_{0.70}Cu_{0.30}Al_2O_4$ composition, bond distances in the tetrahedral site are 4 × 1.938 (3) Å and in the octahedral site 6 × 1.919 (3) Å.

As the copper rate x in the spinel increases, the bond distances between oxygen and cations in the tetrahedral site decrease, whereas the bond distances between oxygen and cations in the octahedral site slightly increase. In Figure 5, the variation of the bond lengths in the both crystallographic sites versus the copper rate x illustrates quite well such evolutions. Actually, this evolution is much more pronounced in the case of the tetrahedral sites ($\Delta d_{Td} = -0.048$ Å; $\Delta d_{Oh} = +0.022$ Å) due to the large amount of Al^{3+} cations in 6-fold coordination which limits the expansion and distortion of octahedral sites.

Table 2. Atomic Positions, Isotropic Thermal Displacements, and Reliability Factors of the Various $Zn_{1-x}Cu_xAl_2O_4$ Compositions (Powder Rietveld Analysis)

atoms	site	*x*	*y*	*z*	biso	occupancies
		$ZnAl_2O_4$ (*Fd*-3*m*), X-ray Refinement, $a = 8.0861(2)$ Å, CRp = 10.6%, CRwp = 14.3%, Rbragg = 4.44				
Zn1/Cu1 8a	1/8	1/8	1/8	0.79 (7)	0.967 (3)	
Al1	8a	1/8	1/8	1/8	0.79 (7)	0.033 (3)
Cu2	16d	1/2	1/2	1/2	0.79 (10)	0.016 (2)
Al2	16d	1/2	1/2	1/2	0.79 (10)	0.984 (2)
O	32e	0.2649 (3)	0.2649 (3)	0.2649 (3)	0.74 (14)	1
		$Zn_{0.90}Cu_{0.10}Al_2O_4$ (*Fd*-3*m*), X-ray Refinement, $a = 8.0851$ (3) Å, CRp = 9.59%, CRwp = 11.5%, Rbragg = 1.67				
Zn1/Cu1 8a	1/8	1/8	1/8	0.691 (40)	0.950 (2)	
Al1	8a	1/8	1/8	1/8	0.691 (40)	0.050 (2)
Cu2	16d	1/2	1/2	1/2	0.651 (67)	0.025 (2)
Al2	16d	1/2	1/2	1/2	0.651 (67)	0.975 (2)
O	32e	0.2639 (2)	0.2639 (2)	0.2639 (2)	0.57 (9)	1
		$Zn_{0.70}Cu_{0.30}Al_2O_4$ (*Fd*-3*m*), X-ray Refinement, $a = 8.0849$ (2) Å, CRp = 13.6%, CRwp = 12.0%, Rbragg = 2.43				
Zn1/Cu1 8a	1/8	1/8	1/8	0.761 (49)	0.846 (8)	
Al1	8a	1/8	1/8	1/8	0.761 (49)	0.154 (8)
Cu2	16d	1/2	1/2	1/2	0.681 (73)	0.077 (4)
Al2	16d	1/2	1/2	1/2	0.681 (73)	0.923 (4)
O	32e	0.2634 (3)	0.2634 (3)	0.2634 (3)	0.81 (10)	1
		$Zn_{0.30}Cu_{0.70}Al_2O_4$ (*Fd*-3*m*), X-ray Refinement, $a = 8.0818$ (2) Å, CRp = 16.3%, CRwp = 11.6%, Rbragg = 3.11				
Zn1/Cu1 8a	1/8	1/8	1/8	0.786 (50)	0.723 (6)	
Al1	8a	1/8	1/8	1/8	0.786 (50)	0.277 (6)
Cu2	16d	1/2	1/2	1/2	0.945 (64)	0.139 (3)
Al2	16d	1/2	1/2	1/2	0.945 (64)	0.861 (3)
O	32e	0.2619 (3)	0.2619 (3)	0.2619 (3)	1.251 (93)	1
		$CuAl_2O_4$ (*Fd*-3*m*), X-ray Refinement, $a = 8.0784$ (2) Å, CRp = 19.9%, CRwp = 13.2%, Rbragg = 3.79				
Cu1	8a	1/8	1/8	1/8	1.030 (65)	0.646 (6)
Al1	8a	1/8	1/8	1/8	1.030 (65)	0.354 (6)
Cu2	16d	1/2	1/2	1/2	0.953 (72)	0.178 (3)
Al2	16d	1/2	1/2	1/2	0.953 (72)	0.822 (3)
O	32e	0.2608 (3)	0.2608 (3)	0.2608 (3)	1.47 (11)	1

Table 3. Calculated and Experimental Intensity and Structure Factors Ratios (400 and 331 Reflections) for $Zn_{0.70}Cu_{0.30}Al_2O_4$ Composition

		simulation		
	exptl	$\gamma = 15\%$	$\gamma = 12\%$	$\gamma = 18\%$
I_{400}/I_{331}	2.10	1.91	1.68	2.23
F_{400}/F_{331}	6.52	6.27	5.52	7.33
ΔF	0	−3.4%	−15.3%	+12.4%

Finally one should have to note that for $Zn_{1-x}Cu_xAl_2O_4$ oxides prepared at low temperatures from metallic salts, only pure spinel compositions with $x < 0.30$ have been obtained by this preparative method.[11]

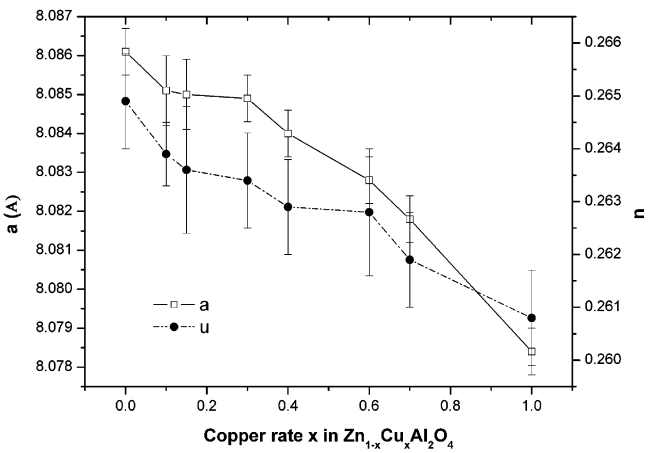

Figure 3. Evolution of the *a* lattice parameter and the *u* oxygen coordinate of the $Zn_{1-x}Cu_xAl_2O_4$ series versus the copper rate.

2. Definition of Two Critical Parameters in the Spinel Network Relating to the Cu^{2+} Local Jahn−Teller Distortion Affecting Tetrahedral and Octahedral Sites. In fact, two critical areas can be identified according to the Figures 3−5. First, for $0 < x < 0.15-0.20$, the *a* parameter seems to be constant (Figure 3) as the *u* oxygen parameter or coordinate undergoes strong variations in this composition range despite the standard deviation values. Second, for $x > 0.60$, a stronger decrease of the a lattice parameter versus *x* Cu content is observed as well as a plateau following by a smaller increasing (Figure 4) in the variation of the

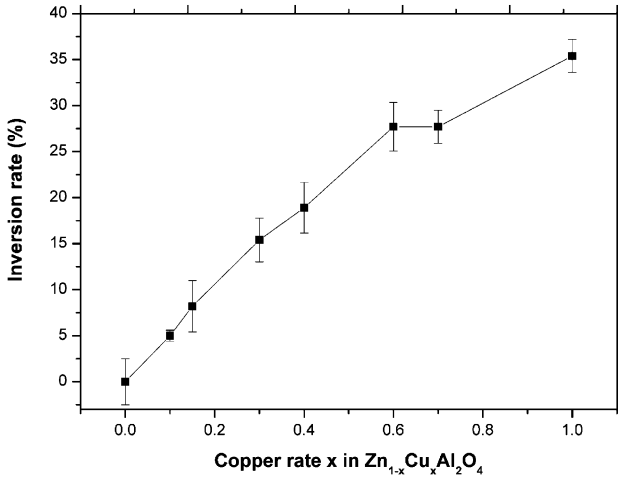

Figure 4. Evolution of the γ inversion rate versus the *x* copper rate.

Table 4. Interatomic Bond Distances in $Zn_{1-x}Cu_xAl_2O_4$ Compositions

$x = 0$			
Zn1-O	1.949 (4)	Al1-O	1.914 (4)
$x = 0.10$			
Zn1/Cu1/Al1-O	1.946 (2)	Al2/Cu2-O	1.915 (2)
$x = 0.30$			
Zn1/Cu1/Al1-O	1.938 (3)	Al2/Cu2-O	1.919 (3)
$x = 0.70$			
Zn1/Cu1/Al1-O	1.917 (2)	Al2/Cu2-O	1.929 (2)
$x = 1.00$			
Zn1/Cu1/Al1-O	1.901 (3)	Al2/Cu2-O	1.936 (3)

inversion rate around this second critical point ($x = 0.60$) despite the standard deviation values. As far as the second region is concerned, after $x = 0.60$, the decreasing of the Cu−O bond distances in tetrahedral sites is accentuated. These evolutions can be interpreted by taking into account the electronic and steric effects of the Jahn−Teller (JT) distortion affecting the first tetrahedral and octahedral neighbors of an octahedral site occupied by a Cu^{2+} cation. Indeed, two main consequences result from the JT distortion. First, an unequal electron distribution should be observed in the octahedral site with local distortion and must affect other tetrahedral and octahedral sites leading to high repulsion and attraction phenomena on the first neighbors. Second, the geometric distortion should imply a self-rearrangement of the structure around the distorted octahedron to preserve the cubic symmetry.

The Jahn−Teller effect related to copper cations ($3d^9$) can be considered as the main feature at the origin of the limited inversion rate observed for the pure $CuAl_2O_4$ spinel. The inversion rate for the pure copper aluminate spinel tends to 35%, which is amazing because of the well-known preference of copper cations for octahedral coordination. The energy difference between tetrahedral and octahedral coordination for Cu^{2+} cations has been indeed estimated to 60 KJ·mol^{-1} to the benefit of octahedral coordination.[15] The cfc network of oxygens can only support a limited cooperative distortion, so that the inversion rate tends to its maximum around 35% in order to limit the number of octahedral sites supporting a Jahn−Teller distortion. Higher inversion rates would give rise to a reduction of the cubic symmetry[7,8] and probably a collapse of spinel network.

For high copper contents ($x > 0.60$), the plateau observed in this region for the inversion rate and the smaller increasing with x suggest that the preferential coordination of copper cations Cu^{2+} switches from the 6-fold coordination toward the 4-fold coordination, since even if the copper rate x in $Zn_{1-x}Cu_xAl_2O_4$ raises, the inversion rate does not increase proportionally. In the same region, the strong decreasing of the average bond distances in tetrahedral site for $x > 0.60$ shows that number of Cu^{2+} cations occupying tetrahedral sites (8a) substituting Zn^{2+} and Al^{3+} ions becomes more and more important associated with an increasing of covalency. After the plateau, as the x Cu content increases, the γ inversion rate raises slowly leading to consider that the maximum constrains are reached. This edge in the structural features evolution can be explained by taking into account

(15) Grimes, R. W.; Anderson, A. B.; Heuer, A. H. *J. Am. Chem. Soc.* **1989**, *111*, 1−7.

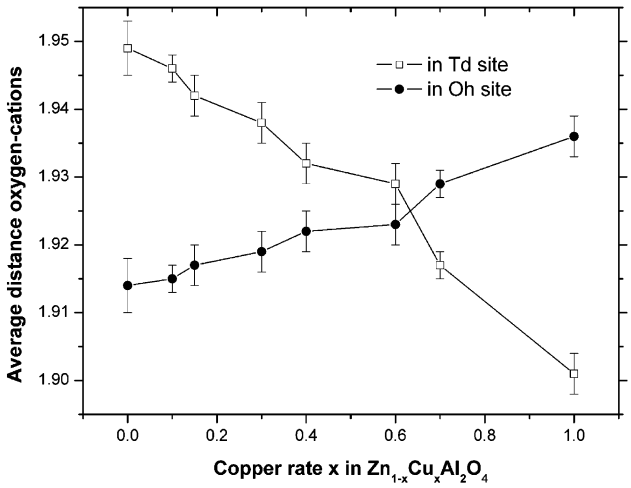

Figure 5. Evolution of the interatomic distances in tetrahedral and octahedral sites versus the copper rate.

the nearest neighbors of one octahedral site in the spinel network. The network arrangement shows that any octahedral site is sharing edges with six other octahedral sites (see Figure 1c) which can be considered as first neighbors. The following description has to be considered on the basis of only isolated JT octahedral site. The structure is so done that one octahedral site exhibiting the Jahn−Teller distortion affects directly six other ones. Finally, as the x copper content reaches the $x = 0.60$ critical composition which is close to the $x = 4/7$ composition, the inversion rate is around 30% corresponding to copper cations half distributed between 8a and 16d sites considering that zinc cations occupy tetrahedral sites. Then, the spinel's formula can be described as follows: $(Zn_{3/7}Cu_{2/7}Al_{2/7})_{Td}[Cu_{2/7}Al_{12/7}]_{Oh}O_4$. It means that 1/7 of the available octahedral sites are occupied by copper cations and affect all the six others octahedral neighbors, considering isolated Cu^{2+} distorted entities. Above this critical composition, the number of divalent copper cations occupying octahedral sites remains limited to values close to 2/7. Then, the additional copper cations are preferentially located in tetrahedral sites in order to limit such a distortion. These structural considerations allow for the explanation of the evolution of the γ inversion rate in the $x > 0.60$ region.

If two copper cations are considered to be nearest neighbors in octahedral sites, the ten surrounding octahedral sites are affected by the JT effect of these two copper cations. In these conditions, for $x = 4/5 = 0.80$, the spinel's formula should be described as follows considering Cu^{2+} ions are half distributed in 8a and 16d sites: $(Zn_{1/5}Cu_{2/5}Al_{2/5})_{Td}$-$[Cu_{2/5}Al_{8/5}]_{Oh}O_4$. In this latter hypothesis, for $x = 4/5$, all octahedral sites should be affected by the local JT distortion of Cu^{2+} pairs. According to experimental data (lattice parameter, inversion rate, and bond distances), one can consider that the critical point is comprised between $x = 4/7$ and $x = 4/5$ but closer to $x = 4/7$ corresponding to isolated Cu^{2+} ions in octahedral sites. The rapid decreasing of the Cu−O bond distances in tetrahedral sites starting from $x = 4/7$ and relating to the increasing of the rate of Cu^{2+} cations in tetrahedral sites is indeed a good argument to consider that the critical zone is around $x = 4/7$.

As far as the evolution of the structural features in the other critical area is concerned, for $Zn_{1-x}Cu_xAl_2O_4$ with $0 < x < 0.15-0.20$ compositions where the *a* lattice parameter seems to exhibit no clear variation despite the standard deviation values, it can be also interpreted as a consequence of the electronic effects associated with the JT distortion observed for copper cations located in octahedral sites.

As previously mentioned, if the environment of one tetrahedral site in the spinel network is considered, one should have to note that each tetrahedral site is directly surrounded by 12 octahedral sites (three at each vertices). Consequently, considering isolated Cu^{2+} entities, for one octahedral site over 12 octahedral sites occupied by one Cu^{2+} cation, all the tetrahedra of the network are touched by the Cu^{2+} in 6-fold coordination and the local JT distortion. Cu^{2+} Jahn−Teller effects in the octahedral environment is stronger, leading to the stabilization of π_{xz}, π_{yz} bands, the destabilization of the $\sigma_{x^2-y^2}$ orbital, and the strong distortion of the octahedral site. For compositions with $x \approx 0.15-0.20 \approx 1/6$, by considering that copper cations are half distributed between 8a and 16d sites thanks the γ refined inversion rate, the spinel's formula can be described as follows: $(Zn_{5/6}Cu_{1/12}Al_{1/12})_{Td}[Cu_{1/12}Al_{23/12}]_{Oh}O_4$. In these conditions, the strong electronic effects associated with the JT distortion in the octahedral site have affected the totality of tetrahedral sites where the deformation remains smaller. Above this second critical composition ($x = 1/6$), electronic effects favorable to Cu^{2+} in octahedral symmetry are no more predominant, but steric considerations have to be taken into account leading to stabilize a large amount of Cu^{2+} cations in tetrahedral coordination. Moreover, for compositions with $x > 1/6$, the probability to get Cu^{2+} ions located in octahedral site organized in pairs with another Cu^{2+} in tetrahedral site becomes high. The *a* cell parameter does not vary with *x* Cu content around the $x = 1/6$ critical composition because the increasing of the unit cell volume due to the occurrence of larger JT Cu^{2+} in the distorted octahedral site is totally compensated by the presence of the Cu^{2+} ion in tetrahedral coordination which occupies a smaller site than Zn^{2+} ions.

In the case of compounds prepared at low temperatures from metallic salts for $0 < x < 0.30$, not only the *a* cell parameter seems to pass through a maximum around $x = 0.15$ near 1/6 but also a plateau can be considered in this region.[11] Then the occurrence of Cu pairs with Cu^+ in tetrahedral sites and Cu^{2+} in distorted octahedral environments have been considered in order to explain the evolution of structural features correlated to optical absorption properties.[11]

Finally, the structure organizes itself in order to limit the local Jahn−Teller distortion and the XRD-refinements giving global or average atomic arrangement indicate that the octahedral and tetrahedral environments for any compositions are almost isotropic and regular. In order to prove the local Jahn−Teller octahedral distortion, electronic spin resonance (ESR) experiments have been undertaken for the low *x* copper contents.

3. The Jahn−Teller Effect of Cu^{2+} in $Zn_{1-x}Cu_xAl_2O_4$ Spinel: An ESR Study. The local environments of Cu^{2+} cations have been determined by ESR measurements (Figure 6) at room temperature and at $T = 5$ K for compositions containing the smaller amounts of copper and for the reference MgO:Cu (2%) compound. For $x = 0.05$ a typical signal relating to Cu^{2+} in the octahedral site has been detected, showing an anisotropic orthorhombic site's distortion ($2 + 2 + 2$; D_{2h} point group) due to the Jahn−Teller effect of Cu^{2+} and a hyperfine structure due to the interaction between an unpaired electron and a Cu nucleus ($I = 3/2$). For $x = 0.15$, the hyperfine structure is strongly attenuated, and the signal is less asymmetric because of the strong evolution of the hyperfine interaction as confirmed by the following simulations. On the other hand, the reference sample (Cu-doped MgO) containing Cu^{2+} cations in octahedral sites exhibits a strong quasi-isotropic ESR signal relative to Cu^{2+} in almost regular octahedral environments without a hyperfine structure (Figure 6e,f). Simulations have given rise to the determination of the *g* values and the hyperfine structure constants of the ESR signals of the zinc−copper aluminate spinels as well as for the reference MgO:Cu compound (Table 5 and Figure 7). One should have to notice the absence of the ESR signal relative to Cu^{2+} in the tetrahedral site. Actually, such an ESR signal would appear with a rather small intensity compared to the signal of the Cu^{2+} cation in octahedral symmetry due to the strong $L + S = 5/2$ spin−orbit coupling, whereas it corresponds to a spin-only $S = 1/2$ situation for Cu^{2+} in the octahedral site.

Whatever the copper content in the various compositions, one should have to note that the *g* values remain almost identical and the octahedral orthorhombic distortion is not affected. Starting from these *g* values, electronic transitions can be deduced: $\Delta_{1,1} = 2\lambda/(g_\perp - g_e)$; $\Delta_2 = 8\lambda/(g_{//} - g_e)$, with g_e being the *g* value for isolated electron ($g_e \approx 2$) and λ the spin−orbit coupling constant of the copper element[16] ($\lambda_{Cu} \approx 830$ cm^{-1}). If $g_{//} = g_z = 2.335$ and $g_\perp = 1/2(g_x + g_y) = 2.104$ are considered as it is the case in Figure 6 (except for MgO:Cu), optical transitions are expected at around $\Delta_{1,1} = 16\,040$ cm^{-1} (620 nm) and around $\Delta_2 = 19\,820$ cm^{-1} (500 nm), and these respective values will be discussed in the final part devoted to optical absorption properties.

ESR measurements confirm also that for low copper content ($x < 0.20$), Cu^{2+} cations adopt a distorted octahedral coordination (Jahn−Teller effect). Cu^{2+} cations are isolated enough from one another because of the large amount of Al^{3+} ions in the octahedral sites, so each Cu nucleus ($I = 3/2$) interacts with its unpaired electron giving rise to a well-defined hyperfine structure. These hyperfine interactions mean that an electronic density appears on the Cu orbital with an s character. The hyperfine constants values (A_x, A_y, A_z) correspond to classical nuclear Zeeman interactions (10^{-3} cm^{-1} or a multiple of 10G). A_x, A_y, and A_z are proportional to the $\psi^2_n(0)$ unpaired spin density on the nucleus and are originated from the symmetry mixing of s orbitals into the ground state ($3d^9$) wavefunction or from spin polarization in the case of s orbitals. One should have to point out that in the case of MgO:Cu where Cu−O bond distances are

(16) Abragam, A.; Bleaney, B. *Electron paramagnetic resonance of transition ions*; Dover Publications: 1986.

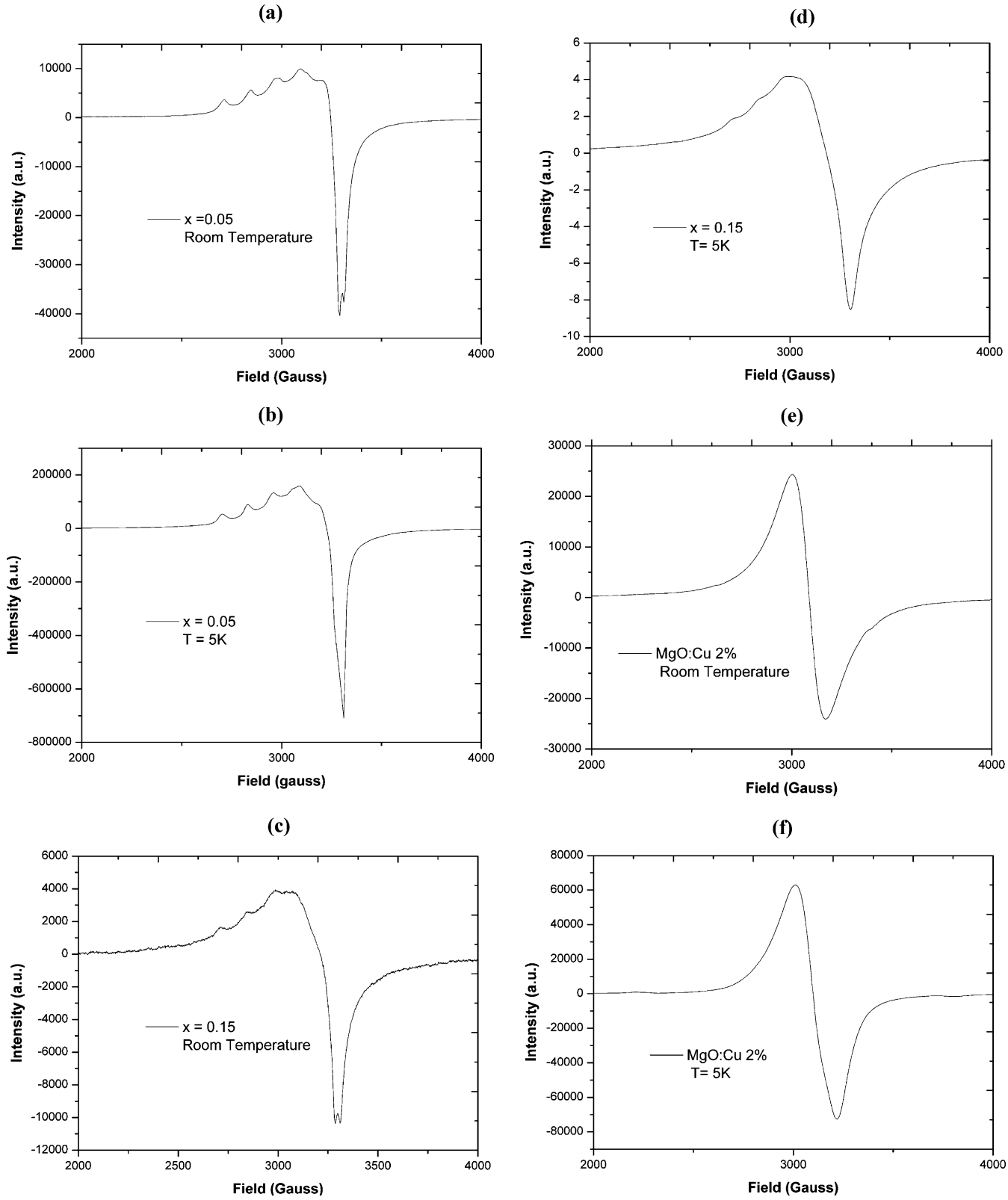

Figure 6. ESR signal at room temperature and at $T = 5$ K for $x = 0.05$ (a, b), $x = 0.15$ (c,d), and MgO (reference; e,f).

around 2.11 Å in this rocksalt type structure instead of 1.92 Å in the spinel ones, the hyperfine structure does not appear at $T = 5$ K. Then, this peculiar feature is probably associated with the strong Cu−O covalency in the $Zn_{1-x}Cu_xAl_2O_4$ spinel network where Cu^{2+} ions occupy partially distorted octahedral sites leading to a configuration interaction between 4s and 3d orbitals. As the copper content increases, the signal around 3200 G, from the most intense peak to the other one, becomes more and more low, and the hyperfine structure tends to be attenuated. Above $x > 0.20$, the signals are broadened, and the hyperfine structure has disappeared because antiferromagnetic Cu^{2+}−Cu^{2+} interactions are too

Table 5. ESR Constants Obtained by Simulation (Simfonia) of the Various Experimental ESR Signals Recorded at $T = 5$ K

	g values			hyperfine structure constants (G)			signal width (G)		
	g_x	g_y	g_z	A_{xx}	A_{yy}	A_{zz}	W_x	W_y	W_z
$Zn_{0.95}Cu_{0.05}Al_2O_4$	2.072	2.135	2.335	5	67	125	20	50	45
$Zn_{0.85}Cu_{0.15}Al_2O_4$	2.072	2.135	2.335	20	70	130	70	110	105
MgO:Cu (2%)	2.110	2.190	2.190				150	150	150

strong. Magnetic measurements have been performed confirming the Curie−Weiss ($\chi = C/(T + \theta_p)$) paramagnetic law (Figure 8) and the increase of $\theta_p = J/k_B$ values (Table 6) versus x content where J denotes the absolute value of the exchange integral due to antiferromagnetic interactions between several Cu^{2+} cations.

Finally in the case of oxides prepared from metallic salts at low temperature, the ESR signal of $x = 0.15$ composition looks like the $x = 0.10$ composition obtained by the solid-state route at high temperature. Thus, by this preparative method leading to the formation of nanoparticles, the Cu^{2+} rate, confirmed by magnetic measurements, is always lower than the total copper content because of the stabilization of Cu^{+I}/Cu^{+II} valence states in this series.[11]

In order to identify the impact of steric and electronic effects associated with Cu^{2+} JT distortion in the $Zn_{1-x}Cu_xAl_2O_4$ series on electronic properties and transitions, the UV−vis-NIR optical absorption properties have been investigated and finally correlated to structural features.

4. Optical Absorption Properties of the $Zn_{1-x}Cu_xAl_2O_4$ Compositions in the UV−Visible-NIR Range and Correlation with Structural Features. Coloration of each composition evolves gradually from white for pure $ZnAl_2O_4$ to brownish-red for pure $CuAl_2O_4$, with intermediate colors as pale green for $x = 0.10$ and pale brown for $x = 0.30$. The UV−visible-NIR spectra reveal the same absorption bands for any spinel containing copper but with various intensities and a slight shift.

UV−visible-NIR absorption properties of the zinc−copper aluminate spinels have been measured by diffuse reflectance spectroscopy and are illustrated in Figures 9 and 10. As the average particle size obtained by a conventional solid-sate route is largely superior to the wavelengths used for the UV−vis-NIR spectroscopy, diffusion and absorption do not vary anymore as a function of particles size, and diffusion can be considered as a low constant parameter. In these conditions, absorption spectra can be deduced from the reflectance spectra by the Kubelka−Munk correction ($A = K/S = (1-R)^2/2R$).[17,18]

The reference compound $ZnAl_2O_4$ displays one absorption band in the UV range, with a band gap determined around 250 nm on the basis of absorption spectra (Figure 9, curve a) which is assigned to a charge-transfer band (CTB) between 2p (oxygen) and 4s (zinc) bands.

As the copper is introduced into the spinel network, several absorption bands in addition to O−Zn CTB appear at 450, between 550 and 1000 nm, and between 1100 and 1900 nm, whose intensities increase with the x copper content. The bands at 260 and 450 nm are related to charge transfers between 2p oxygen orbitals and 4s bands of Zn^{2+}/Cu^{2+} ions and 3d orbitals of Cu^{2+}, respectively. Indeed, for high copper content, the charge-transfer corresponding to the band

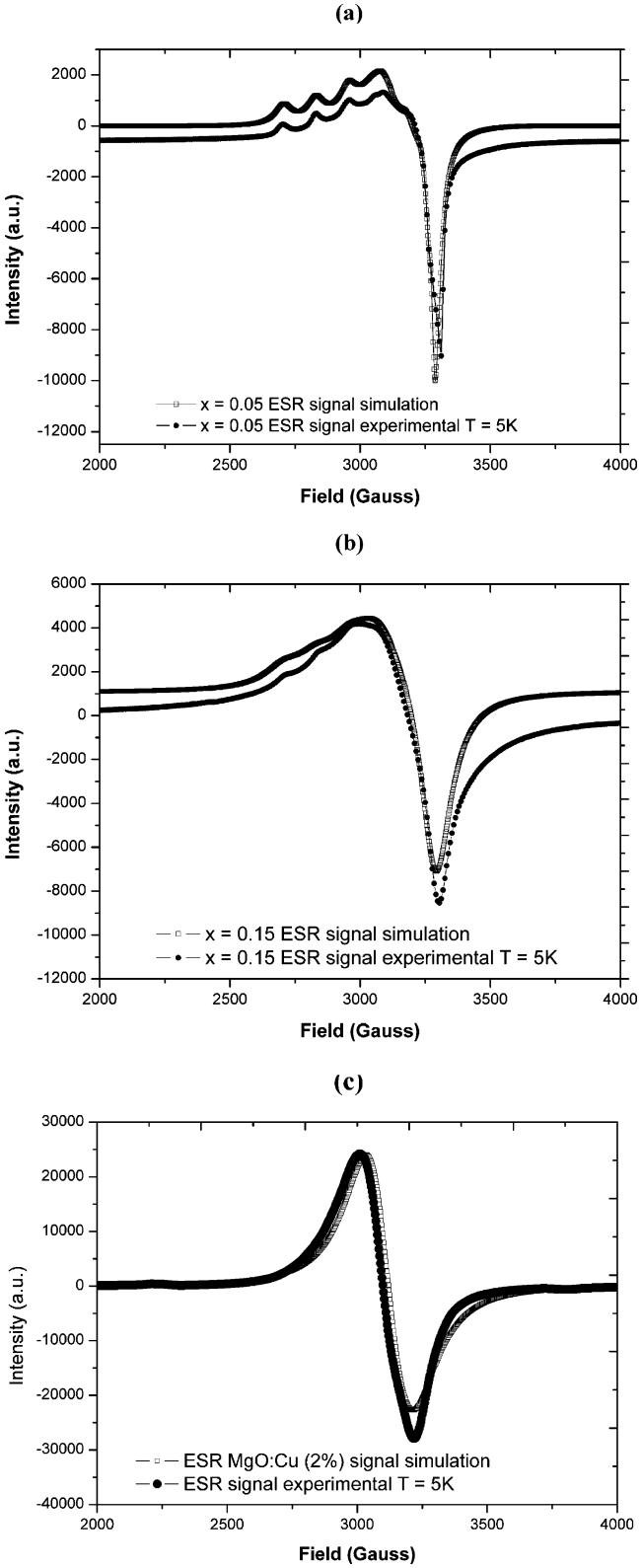

Figure 7. Simulated ESR signals for $x = 0.05$ (a); $x = 0.15$ (b) compositions and MgO:Cu compounds (c).

(17) Kubelka, P.; Munk, F. *Z. Tech. Phys.* **1931**, *11*, 593−600.
(18) Kubelka, P. *J. Opt. Soc. Am.* **1948**, *38*, 448−457.

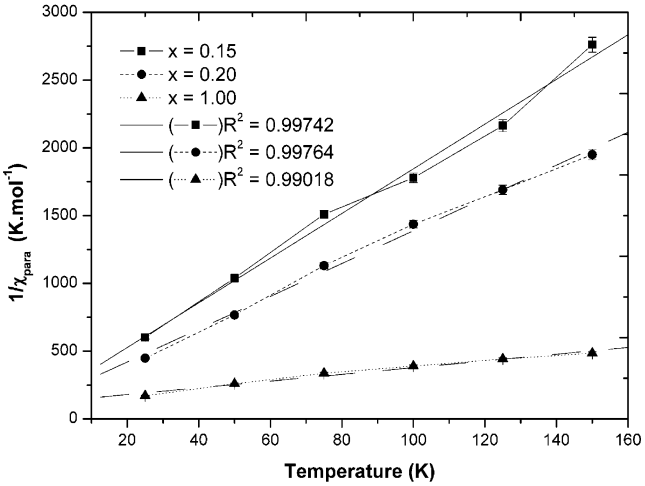

Figure 8. Evolution of the magnetic susceptibility inverse versus temperature for $x = 0.15$, $x = 0.20$, and $x = 1.00$ compositions.

Table 6. Curie Constants and *J*/*k* Values Determined on the Basis of Susceptibility Inverse Variation versus Temperature

x in $Zn_{1-x}Cu_xAl_2O_4$	0.15	1
J/k_B	19.3 (2)	67.1 (5)
C (mol^{-1})[a]	0.0661 (5)	0.4507 (9)

[a] On the basis of $g = (g_x + g_y + g_z)^{1/3} \approx 2.183$, the Curie constant for copper element can be estimated to $C = 1/8 \cdot g^2 \cdot S(S+1) = 0.4470$ mol^{-1} with $S = 1/2$ (case of d^9 element).

centered at around 450 nm is strongly dependent on the relative position of the valence band and the empty 3d copper orbitals, t_2 or e according to the various environments. It is reasonable to consider in a first hypothesis that the charge transfer between oxygen and copper cations in octahedral coordination takes place at higher energy than the transfer between oxygen and copper cations in the tetrahedral environment, since the octahedral ligand field is higher than the tetrahedral one. Moreover, it seems that the charge-transfer band identified in the case of $ZnAl_2O_4$ is shifted toward the lower energy after copper introduction in the matrix. Furthermore, the comparison of ZnO:Cu and MgO:Cu absorption spectra (Figure 11) confirms that CTB are shifted to higher wavelengths in relation to pure oxides. In an ionic compound such as MgO, the CTB involving Cu^{2+} in the octahedral environment seems to appear in the same energy range (around 400 nm) as the CTB implying Cu^{2+} in the tetrahedral site in ZnO which can be considered as an iono-covalent oxide despite the drastic shift of the global CTB edge in the ZnO matrix associated with the increase of the covalency. Assignment of the various charge-transfer bands will be discussed later on the basis of several structural considerations.

The two absorption bands between 550 and 1000 nm and between 1100 and 1900 nm can be attributed to intra-atomic d−d transitions associated with copper in octahedral and tetrahedral sites, respectively, and those assignments are in good agreement with the literature.[19−24] Moreover, the ligand

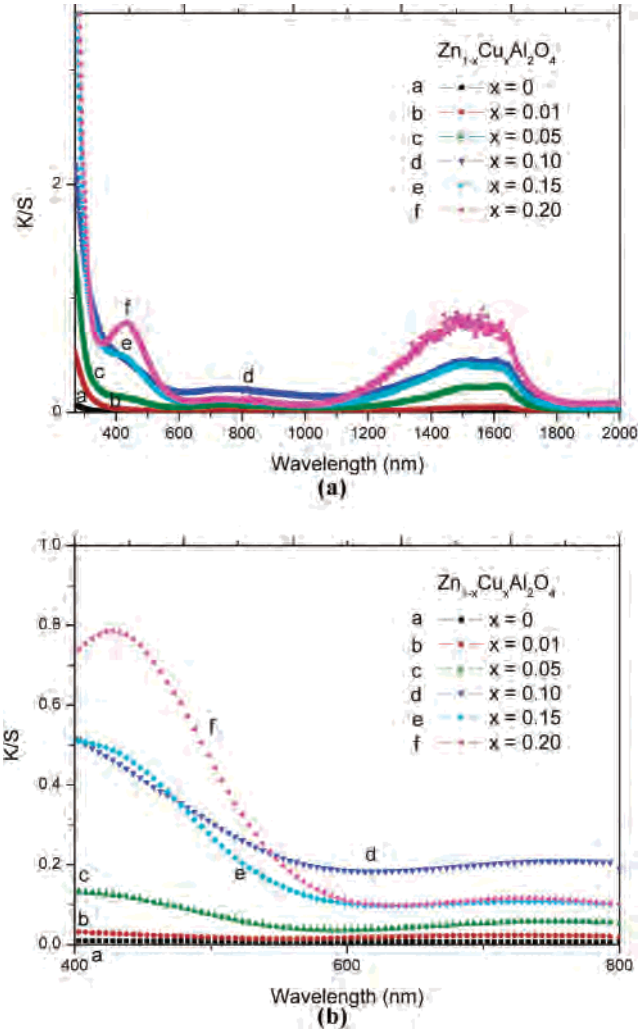

Figure 9. UV−vis-NIR absorption properties of the $Zn_{1-x}Cu_xAl_2O_4$ series for $0 \le x \le 0.20$ (a) and zone enlargement to the visible range (b).

field values deduced from the energy corresponding to the two absorption bands ($\Delta_{Td}/\Delta_{Oh} = 750/1550 \approx 0.48$) agree with the theoretical relationship $\Delta_{Td} = 4/9\Delta_{Oh}$. Moreover synthesis of reference compounds such as ZnO:Cu for Cu^{2+} in tetrahedral coordination and MgO:Cu for Cu^{2+} in octahedral coordination has confirmed the average positions of the absorption bands relative to d−d transitions due to Cu^{2+} in one or the other environment (Figure 11). Although d−d transitions associated with Cu^{2+} in the tetrahedral site appear in the NIR range around 1500 nm, it is nevertheless clear that d−s transitions should occur in a close region corresponding to an energy close to 1 eV (1250 nm). Moreover, in the case of the noncentrosymmetric site such as the tetrahedral environment, the d−d or d−s transitions are allowed despite the $\Delta L = 0$ or 2 values, whereas these transitions are forbidden for centrosymmetric octahedral sites.

(19) Rodriguez, F.; Hernandez, D.; Garcia-Jaca, J.; Ehrenberg, H.; Weitzel, H. *Phys. Rev. B: Condens. Matter Mater. Phys.* **2000**, *61*, 16 497−16 501.
(20) Pappalardo, R. *J. Mol. Spectrosc.* **1961**, *6*, 554−571.
(21) El Jazouli, A.; Alami, M.; Brochu, R.; Dance, J. M.; Le Flem, G.; Hagenmuller, P. *J. Solid State Chem.* **1987**, *71*, 444−450.
(22) Duan, X. L.; Yuan, D. R.; Xu, D.; Lu, M. K.; Wang, X. Q.; Sun, Z. H.; Wang, Z. M.; Sun, H. Q.; Lu, Y. Q. *Mater. Res. Bull.* **2003**, *38*, 705−711.
(23) Duan, X.; Yuan, D.; Cheng, X.; Luan, C.; Sun, Z.; Wei, X.; Guo, S.; Xu, D.; Lv, M. *Inorg. Chem. Commun.* **2004**, *7*, 62−64.
(24) Dean, P. J.; Robbins, D. J.; Bishop, S. G.; Savage, J. A.; Porteous, P. *J. Phys. C: Solid St. Phys.* **1981**, *14*, 2847−2858.

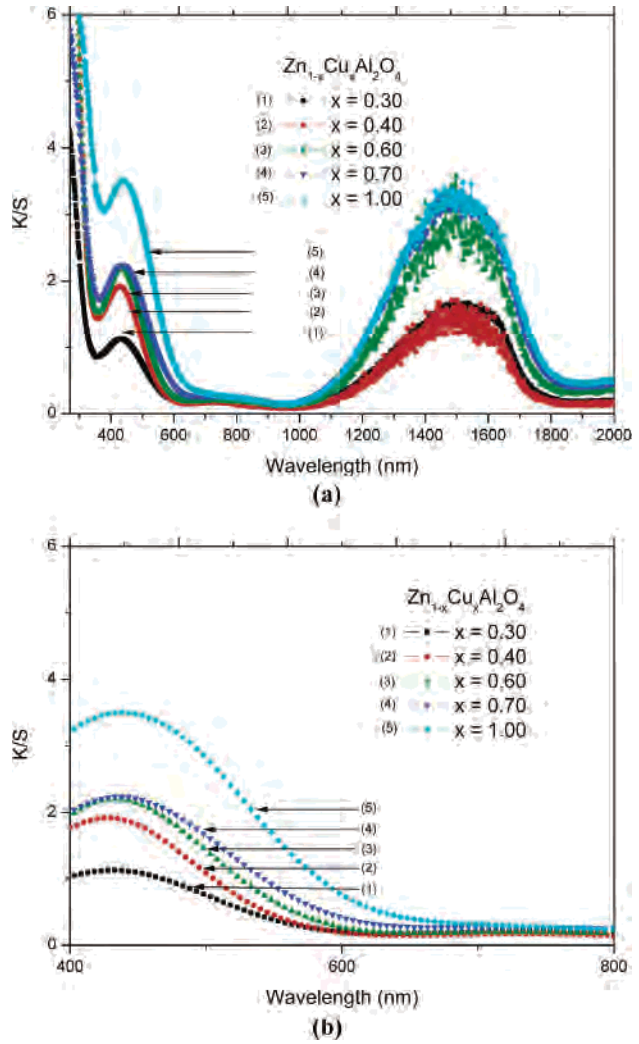

Figure 10. UV−vis-NIR absorption properties of the $Zn_{1-x}Cu_xAl_2O_4$ series for $0.30 \leq x \leq 1.00$ (a) and zone enlargement to the visible range (b).

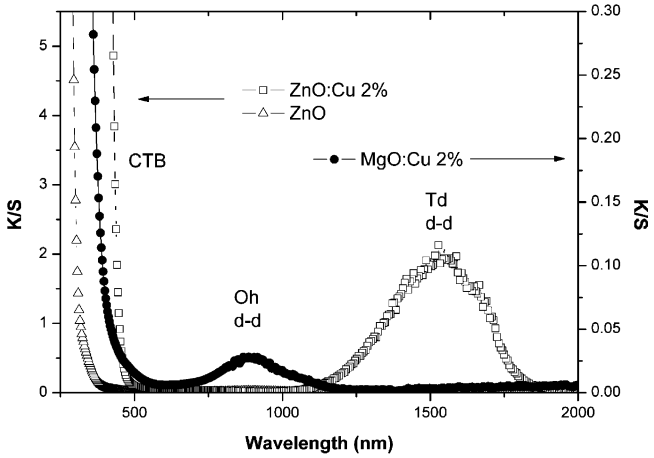

Figure 11. Absorption band spectra of zinc oxide, copper-doped zinc oxide (reference for Cu^{2+} in tetrahedral site), and copper-doped magnesium oxide (reference for Cu^{2+} in octahedral site) (pure magnesium oxide is not represented since it is used as a reference).

Because of the appearance of hyperfine structure on ESR spectra leading to consider the occurrence of electron with s character, a high dispersion of s orbitals and the covalent feature of copper can be proposed in Zn-based oxides. Then, the bands in the NIR region can be attributed both to d−d and d−s transitions of Cu^{2+} with tetrahedral ligand field in zinc oxide and zinc−copper aluminate spinels because of the covalent character of Cu−O chemical bonding in theses oxides.

The two CTB around 260 and 450 nm are doubtless correlated to the presence of copper in the network, since the second CTB around 450 nm appears when copper is introduced into the matrix and since the first CTB observed for $ZnAl_2O_4$ and which implies the 2p levels of oxygen and the 4s band of zinc is shifted toward the lower wavelengths. As mentioned previously, a first approach consists of assigning each transition to a ligand field effect for copper. Then, the first charge transfer should concern the oxygen orbitals and the empty d orbitals of copper in the octahedral environment. Then the second one should be assigned to an electronic transfer O ($2p^6$) → Cu^{2+} ($e^4t_2^5$, tetrahedral site). Nevertheless, the energy difference observed between these two electronic transitions are not in good agreement with the theoretical shift between the Cu empty d orbitals corresponding to each environment. Actually, this energetic shift should be close to 19/45 Δ_{Oh} ($\Delta E = 3/5\ \Delta_{Oh} - 2/5\ \Delta_{Td}$, $\Delta_{Td} = 4/9\ \Delta_{Oh}$), i.e. 0.7 eV if $\Delta_{Oh} = 1.6$ eV on the basis of the d−d transition band at around 750 nm assigned to Cu^{2+} ions in octahedral sites. With an experimental point of view, both charge-transfer bands are separated from 1.7 eV, and this difference is too high to imply the two 3d levels correspond to octahedral and tetrahedral sites, respectively.

The first CTB involves probably the s band of Zn and Cu if we consider that s and d levels are separated from 1 eV. Then, as discussed in the case of CTB in ZnO:Cu and MgO:Cu oxides, the CTB involving Cu^{2+} both in tetrahedral and octahedral sites should correspond to the second band at 450 nm.

It is interesting to note that the second CTB around 450 nm in the $Zn_{1-x}Cu_xAl_2O_4$ series appears clearly for $x = 0.15-0.20$ corresponding to the first critical zone previously defined ($x = 1/6$). Moreover, a comparison of the evolution of the d−d(s) transitions involving Cu^{2+} in octahedral and tetrahedral sites versus the x Cu content shows for $0 \leq x \leq 0.20$ that the $x = 0.10$ composition exhibits the highest band attributed to d−d transition involving octahedral sites, whereas the highest band associated with tetrahedral sites is observed for $x = 0.20$ composition. Between $x = 0.10$ and $x = 0.20$, the intensity of such intra-atomic transitions evolve drastically. This strong change can be interpreted on the basis of the distortion of octahedral sites associated with the electronic effects of Cu^{2+} JT ions because the inversion rate increases regularly from $x = 0$ to $x = 0.30$ and corresponds to a value close to $x/2$ showing that Cu^{2+} cations remain half distributed between tetrahedral and octahedral sites. Actually below the $x = 1/6$ critical composition, the number of Cu^{2+} ions in octahedral sites more or less isolated and distorted increases regularly as well as the number of Cu^{2+} ions in tetrahedral sites. Above this critical point, the creation of $Cu^{2+}-Cu^{2+}$ pairs in tetrahedral and octahedral environments, as previously mentioned, tends to limit the distortion of octahedral sites and contributes to the increase of the Cu−O bond covalency and to the appearance of strong d−s

intra-atomic transitions around 1300 nm. Moreover the strong increase of the second CTB around 450 nm for $x = 0.20$ composition is in good agreement with the brutal change observed for the intra-atomic transitions associated with the covalent character of Cu^{2+}−Cu^{2+} pairs.

As far as zinc copper aluminates prepared from metallic salts at low temperatures are concerned, the absorption spectrum corresponding to $x = 0.15$ composition exhibits drastic changes associated with the creation of defects, i.e., oxygen vacancies and Cu^{+I}/Cu^{+II} mixed valencies stabilized in the network. Moreover around this x Cu content ($x_1 = 1/6$), the variation of absorption spectra versus the annealing temperature ($T = 700$ °C and $T = 1000$ °C) is the strongest. Actually at $x_1 = 1/6$, a large rate of Cu^{+I}−Cu^{+II} pairs can be stabilized in tetrahedral and distorted octahedral sites, respectively, leading surprisingly to their oxidation at higher temperatures. By this preparative method at low temperatures, the spinel network allows the stabilization of Cu^{2+} JT ions in distorted octahedral sites or 5-fold coordinated environments and Cu^{+} in tetrahedral sites forming Cu^{2+}−Cu^{+} pairs. As previously mentioned, at $x_1 = 1/6$, the number of Cu pairs becomes high, and their stabilization is strong on the electrostatic point of view leading to the creation of oxygen vacancies. An annealing at $T = 1000$ °C contributes to the reduction of oxygen vacancies and then surprisingly to the oxidation of copper:[11] $Cu^{+I} \rightarrow Cu^{+II} + e^{-}$.

For $0.30 \leq x \leq 1.00$, the comparison of the absorption spectra (Figure 10) shows for compositions with $x \geq 0.60$ the CTB bands shift to lower energy, resulting in the covalency increasing. Moreover the d−d(s) intra-atomic bands attributed to Cu^{2+} in tetrahedral sites strongly increases from $x = 0.40$ to $x = 0.60$ and saturates from $x = 0.60$. As previously discussed, above this $x = 4/7$ critical composition, the Jahn−Teller distortions due to the presence of Cu^{2+} cations in octahedral sites become too large because of the strong probability to get Cu^{2+}−Cu^{2+} pairs in both octahedral environments.

The insertion of copper in tetrahedral as well as in octahedral sites results in the increase of the cation-oxygen distances in octahedral sites and in the decrease of these same distances in tetrahedral sites. Globally the copper−oxygen hybridization is enhanced: the σ^* orbitals (empty d orbitals) are destabilized, and the 4s band is stabilized leading to the reduction of the 4s- σ^* (3d) energy differences. Consequently, the optical band gap in the series is reduced. Above the $x = 4/7$ critical composition, copper cations are not allowed to occupy additional octahedral sites on the basis of steric and electronic considerations, and it is the reason why the intra-atomic transition band becomes saturated because of the large number of Cu^{2+} cations in tetrahedral sites. The average cations-oxygen distances in tetrahedral sites reduce themselves more and more because of the occupancy of larger octahedral environments by Cu^{2+} cations. Finally, the evolution of optical absorption bands versus x has been correlated to the occurrence of two critical x values, $x_1 = 1/6$ and $x_2 = 4/7$, relating to the high probability of getting Cu^{2+} ions organized in pairs in tetrahedral/octahedral sites and octahedral/octahedral sites.

Then starting from $x = 1/6$, a strong evolution of Cu−O covalency has to be pointed out due to the creation of $Cu^{2+}{}_{Td}$−$Cu^{2+}{}_{Oh}$ pairs and the relaxation of electronic effects. From $x_2 = 4/7$, because of the steric effects and the too strong interactions between Cu^{2+} ions located in octahedral sites, Cu^{2+} ions are preferentially stabilized in tetrahedral sites.

Conclusion

The study of the $Zn_{1-x}Cu_xAl_2O_4$ compositions reveals the occurrence of a solid solution for $0 \leq x \leq 1$. On the basis of powder XRD data analysis (Rietveld) the evolution of the cell parameter of the spinel structure (SG: *Fd*-3*m*) shows the occurrence of a plateau at around $x_1 = 1/6$ which has been defined as a first critical parameter. For this composition, the probability to get pairs of Cu^{2+}−Cu^{2+} ions both in tetrahedral and octahedral sites becomes high. Then, the large increase in the octahedral site size due to the incorporation of Cu^{2+} JT ions is compensated by the presence of Cu^{2+} ions in the tetrahedral environment and the formation of pairs which allow for keeping the *a* cell parameter quasi-constant.

Another preparative method based on a polyesterification reaction using metallic salts followed by an annealing at low temperatures allows the stabilization of nanoparticles of pure zinc−copper aluminates with $x < 0.30$. The absorption spectra are clearly different from those of homologous compositions obtained by the solid-state route or annealed at higher temperatures because of the occurrence of a large content of defects, i.e., oxygen vacancies associated with Cu^{+I}/Cu^{+II} mixed valence states, for the compositions obtained from low-temperature preparative techniques.[11]

For $x > 0.30$, the *a* parameter decreases regularly, and the γ inversion rate is almost equal to $x/2$ for $x < x_2 = 4/7$ leading to consideration that Cu^{2+} cations are half distributed between tetrahedral and octahedral sites. From $x_2 = 4/7$ the γ inversion rate decreases up to $\gamma = 0.35$ for $CuAl_2O_4$ composition, corresponding to almost 1/3 of Cu^{2+} ions in octahedral sites and 2/3 in tetrahedral sites. In these conditions, one octahedral site over six is the limit rate in good agreement with the fact that each octahedral site shares edges with 6 other octahedral sites, and Cu^{2+} JT distortion in octahedral environment does not grow in the $Zn_{1-x}Cu_xAl_2O_4$ spinel. For this x_2 second critical composition, the probability of getting pairs of Cu^{2+} ions located now in octahedral sites remains high, and the network does not support such constrains and distortion and the preference of Cu^{2+} ions for tetrahedral sites becomes strong. Moreover one should have to notice that the M−O bond distances in tetrahedral sites decrease more strongly from $x_2 = 4/7$.

As far as the optical absorption properties are concerned, the formation of $Cu^{2+}{}_{Td}$−$Cu^{2+}{}_{Oh}$ pairs around the $x_1 = 1/6$ critical composition (comparison between $x = 0.10$ and $x = 0.20$ composition) is clearly emphasized where the charge-transfer band around 450 nm strongly changes and a clear evolution of the intra-atomic d−d(s) transition band is identified. Moreover another change occurs around $x_2 = 4/7$ (comparison between $x = 0.40$ and $x = 0.60$ compositions) where the d−d(s) intra-atomic transition band strongly

increases and saturates due to the preference of Cu^{2+} ions to be located in tetrahedral sites, whereas the O−Cu CTB intensity remains almost identical and is not affected around the x_2 critical composition by the larger proportion of Cu^{2+} ions in tetrahedral sites. This evolution implying various electronic transitions is in good agreement with the increasing of the Cu−O bond covalency leading to consider the occurrence of d−s intra-atomic transitions around 1 eV. Then, the Cu−O CTB evolution illustrates clearly the increasing of the bond covalency associated with the formation of Cu^{2+}_{Td}−Cu^{2+}_{Oh} pairs in a first step and in a second step the creation of Cu^{2+}_{Oh}−Cu^{2+}_{Oh} pairs which are crucial and determining for the evolution of structural features and electronic properties. The identification of critical x_1 and x_2 compositions based on the perturbation of the local environment of tetrahedral and octahedral sites into the spinel network can be generalized to others systems containing highly distorted Jahn−Teller ions.

IC062329C